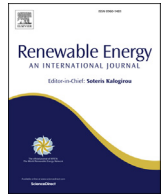




Contents lists available at ScienceDirect

Renewable Energy

journal homepage: [www.elsevier.com/locate/renene](http://www.elsevier.com/locate/renene)

# Sensitivity analysis of homogeneous reactions for thermochemical conversion of biomass in a downdraft gasifier

Umesh Kumar, Manosh C. Paul\*

Systems, Power &amp; Energy Research Division, James Watt School of Engineering, University of Glasgow, Glasgow, G12 8QQ, UK

## ARTICLE INFO

### Article history:

Received 10 May 2019

Received in revised form

14 October 2019

Accepted 8 November 2019

Available online xxx

### Keywords:

Biomass gasification

CFD modelling

Chemical kinetics

Discrete phase model

## ABSTRACT

Biomass containing organic materials could come from a number of sources such as from agricultural residues, sustainable forests, waste food, and industry by-products. Also, being a renewable source of energy, it has the significant potential to reduce greenhouse gas emissions releasing from the fossil fuel based technologies. Therefore, energy from biomass is becoming a favourable technology to convert solid fuel to valuable gas and one of the effective approaches is gasification. In this research, a three dimensional (3D) computational fluid dynamics (CFD) steady-state thermochemical model is developed to simulate biomass (rubber wood) gasification in a downdraft gasifier. Simulated CFD model includes all the four zones (drying, pyrolysis, oxidation and reduction) of gasifier. For optimising the gasifier temperature and syngas composition, a sensitivity analysis of homogeneous oxidation reactions is carried out, with the model identifying the suitable kinetic reactions for gasification. Predicted CFD modelling results are compared with those from the kinetic modelling and experimental results, where a good agreement is obtained. The effect of gasifier temperature, equivalence ratio (ER) and biomass feed rate on the syngas production is studied. Further, the effect of volatile composition and rate of Boudouard reaction at different ERs along the gasifier height is investigated.

© 2019 Elsevier Ltd. All rights reserved.

## 1. Introduction

The world's total energy consumption is estimated to increase from 549 quadrillion Btu in 2012 to 815 quadrillion Btu in 2040. The energy demand has also been expected to increase by 48% by 2040 in line with the increase in the world population and economic development worldwide [1]. However, the energy demand sets against the simultaneous fossil fuels depletion and the widespread concern about the environmental impact of energy conversion systems, well recognised as the main cause of the greenhouse gases emissions. This thus has progressively brought to light the role of renewable energy sources [2,3].

Biomass is one of the trustworthy renewable sources of energy, which could be used for sustainable power and heat generation. Biomass is an alternate source of energy against the gradual depletion of conventional fossil fuels [4]. Biomass gasification is a thermochemical conversion process, which converts solid fuel into useful gaseous (syngas). Partial oxidation process of biomass,

taking place in gasification, results in the production of carbon monoxide, carbon dioxide, hydrogen, and methane. The thermochemical conversion process or syngas quality is affected by the gasifying agent supply such as air, oxygen, steam and mixture of both [6]. It also produces long chain molecules such as tar and inert ash [5].

In the literature, various mathematical models have been developed to investigate the gasification systems on different levels of accuracy and modelling depth. Generally, these mathematical models can be categorised into two parts namely thermodynamic equilibrium and non-equilibrium or kinetic models. Thermodynamic equilibrium modelling technique is based on the maximum yield syngas and equilibrium temperature by assuming that the chemical reactions reach the equilibrium. However, most of the equilibrium model in the literature only considered a single lumped reaction model or considered four zones as a single lumped zone for downdraft gasifier [7–11]. But, in a real chemical reactive system, it is difficult to achieve the equilibrium and these models are independent on the reactor design, therefore these models are only helpful for studying the effect of operating parameters [12]. In addition, an equilibrium model lacks of detailing information inside the gasifier like gas-solid interface, gasifier temperature and

\* Corresponding author.

E-mail address: [Manosh.Paul@glasgow.ac.uk](mailto:Manosh.Paul@glasgow.ac.uk) (M.C. Paul).

concentration profile.

While a non-equilibrium or a kinetic model accounts the chemical and physical properties along the gasifier height by assuming a vertical object, it still lacks in comprehensively understanding and real visualisation of the biomass gasification systems and also the effect of operating parameter and design parameter on the syngas production [13–15]. Therefore, to further progress this research, advanced computational fluid dynamics (CFD) models are required.

A CFD model was developed for gasification of sawdust in entrained gasifier [16]. Two-dimensional (2D) CFD model investigated the gasification systems, however, in this model only the oxidation zone was considered [17]. A three-dimensional model (3D) CFD model was developed for fast pyrolysis of biomass in a fluidized bed reactor. In that study, the main focus was to study the pyrolysis phenomena and impact of operating parameter on the pyrolysis process [18]. Another 2D CFD model was developed for biomass fast pyrolysis in a fluidized bed reactor [19]. Liu et al. [20] established a 3D steady state model to simulate biomass gasification in a circulating fluidized bed (CFB) reactor.

In the literature, a limited number of CFD simulation model for downdraft gasifiers are found. Of particular interest is the two dimensional CFD model for biomass gasification in a downdraft gasifier presented in Ref. [21]. They considered the gasifier as a rectangular two-dimensional geometry, which obviously does not reflect the real structure of a downdraft gasifier. Recently, the authors developed a 2D CFD model for a downdraft gasifier for the gasification of rubber wood feedstock [22,25]. In this study, a volatile break-up approach was used to calculate the volatile fractions from feedstock, and the effect of gasifier temperature and equivalence ratio (ER) on the gas syngas composition was studied [22]. A very few 3D CFD study on biomass gasification in downdraft gasifier is reported in the literature. Further, in the literature, a large number of reaction kinetics published for biomass gasification. Therefore, a detailed kinetic study is initially performed in this work to optimise the reaction kinetics for biomass gasification. Further, an attempt is made to develop a full-scale 3D CFD model for biomass gasification in a downdraft gasifier. In the gasification, chemical kinetics play an important role in developing the computational model. Therefore, several reaction kinetics for the oxidation of carbon monoxide, hydrogen and methane are investigated in predicting the optimum gasifier temperature and syngas composition, backed up by the experimental and other data sourced from the literature. This model has also a crucial role to play in further development of the chemical kinetics research for gasification and be useful for better understanding of the biomass gasification process and its design conditions.

## 2. Model description

Fig. 1 shows a schematic diagram of a downdraft gasifier used for biomass gasification modelling.

The gasifier is divided into four zones namely drying, pyrolysis, oxidation and reduction, which are also shown in Fig. 1. The dimensions as well as design conditions for the gasifier are taken from a recent study that focused on the development of an integrated kinetic model [23]. This kinetic model was tested with experimental results and subsequently, proposed the optimum design parameter for the downdraft gasifier used in this study. Air is injected from the oxidation zone while biomass is feed from the top of the gasifier.

The governing transport equations include the mass conservation, momentum transfer, energy and species concentrations which are solved numerically under the steady-state and turbulent flow conditions with a set of finite rate reaction kinetics as described

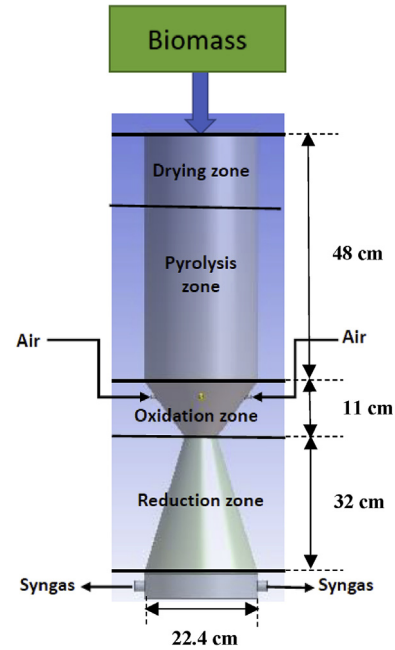


Fig. 1. Schematic of the downdraft gasifier used for biomass gasification.

below.

### 2.1. Mass and momentum conservation equations

The mass and momentum conservation equations respectively given as follows

$$\frac{\partial \rho}{\partial t} + \frac{\partial(\rho u_i)}{\partial x_i} = S_i, \quad (1)$$

where  $\rho$  is the density of fluid,  $u_i$  is the fluid velocity component and  $S_i$  is the mass element added to the continuous phase from the dispersed phase explained in Section 2.3.

$$\frac{\partial(\rho u_i)}{\partial t} + \frac{\partial(\rho u_i u_j)}{\partial x_j} = -\frac{\partial P}{\partial x_j} + \frac{\partial \tau_{ij}}{\partial x_j} + \rho g_i + F_i, \quad (2)$$

where  $g_i$  is the gravitational acceleration,  $P$  is the pressure,  $F_i$  is the external body force and  $\tau_{ij}$  is the stress tensor expressed by the following equation

$$\tau_{ij} = \mu \left[ \left( \frac{\partial u_i}{\partial x_j} + \frac{\partial u_j}{\partial x_i} \right) - \frac{2}{3} \nabla \cdot u_{ij} I \right], \quad (3)$$

where  $\mu$  is the molecular viscosity and  $I$  is the unit tensor that is associated with the effect of any volume dilation.

A Reynolds time-averaging technique is employed to first derive the Reynolds averaged Navier–Stokes (RANS) form of the equations from (1)–(3). The additional Reynolds stresses introduced in those equations are then modelled through the Boussinesq hypothesis depending strongly on the turbulence kinetic energy,  $k$ , and its rate of dissipation,  $\epsilon$ , which are obtained from the following transport equations (standard  $k$ - $\epsilon$  model):

$$\frac{\partial}{\partial x_i} (\rho k u_i) = \frac{\partial}{\partial x_j} \left[ \left( \mu + \frac{\mu_t}{\sigma_k} \right) \frac{\partial k}{\partial x_j} \right] + G_k + G_b - \rho \epsilon - Y_M + S_k. \quad (4)$$

In the above equation,  $\mu_t$  is the turbulent viscosity,  $\sigma_k$  is the

turbulent viscosity,  $G_k$  is the turbulence kinetic energy due to the mean velocity gradients,  $G_b$  is the turbulence kinetic energy due to the buoyancy force,  $Y_M$  is the contribution of the fluctuating dilatation turbulence to the overall dissipation rate, and  $S_k$  is the source term for the kinetic energy.

$$\frac{\partial}{\partial x_i} (\rho \epsilon u_i) = \frac{\partial}{\partial x_j} \left[ \left( \mu + \frac{\mu_t}{\sigma_\epsilon} \right) \frac{\partial \epsilon}{\partial x_j} \right] + C_{1\epsilon} \frac{\epsilon}{k} (G_k + C_{3\epsilon} G_b) - C_{2\epsilon} \rho \frac{\epsilon^2}{k} + S_\epsilon, \quad (5)$$

where  $\sigma_\epsilon$  is the turbulent Prandtl number for  $\epsilon$ , and  $S_\epsilon$  is the source term for the rate of dissipation. In equations (4) and (5), the model parameters used are  $C_{1\epsilon} = 1.44$ ;  $C_{2\epsilon} = 1.92$ ;  $\sigma_k = 1.0$ ;  $\sigma_\epsilon = 1.3$  [24].

## 2.2. Species transport equation

The species transport equation is written as follows

$$\frac{\partial}{\partial t} (\rho Y_i) + \nabla \cdot (\rho \vec{u} Y_i) = -\nabla \cdot \vec{J}_i + R_i + S_i, \quad (6)$$

where  $Y_i$  is the mass fraction of species  $i$ ,  $R_i$  is the net rate of production of species  $i$  by the chemical reaction, and  $J_i$  is the diffusion flux for turbulent flow expressed as

$$\vec{J}_i = - \left( \rho D_{i,m} + \frac{\mu_t}{Sc_t} \right) \nabla Y_i - D_{T,i} \frac{\nabla T}{T}, \quad (7)$$

where  $D_{i,m}$  is the mass diffusion coefficient for species  $i$  in the mixture and  $D_{T,i}$  is the thermal diffusion coefficient for species  $i$ .  $Sc_t$  is the Schmidt number for turbulent flow which is given by the following equation:

$$Sc_t = \frac{\mu_t}{\rho D_t} \quad (8)$$

In the above equation,  $D_t$  is the turbulent diffusivity.

## 2.3. Model for discrete phase

The flow of biomass particles is modelled by a Lagrangian approach namely discrete phase model (DPM). The model considers the trajectory of a particle through the continuous phase of fluid, while their interaction is accounted by considering the heat and mass losses of the particles as a source term in the governing equations. The trajectory of a discrete phase particle is written in a Lagrangian reference frame by integrating the force balance on the particle. This force balance equates the particle inertia with the forces acting on the particle as described by the following equation:

$$\frac{\partial \vec{u}_p}{\partial t} = F_D (\vec{u} - \vec{u}_p) + \frac{\vec{g} (\rho_p - \rho)}{\rho_p}, \quad (9)$$

where  $\vec{u}_p$  is the particle velocity,  $F_D (\vec{u} - \vec{u}_p)$  is the drag force per unit particle mass,  $\rho_p$  is the density of particle, and  $F_D$  is the drag force determined by

$$F_D = \frac{18 \mu C_D Re}{24 \rho_p d_p^2}, \quad (10)$$

where  $C_D$  is the drag coefficient, and the flow Reynolds number ( $Re$ ) is derived by the following equation:

$$Re = \frac{\rho d_p |u - u_p|}{\mu}. \quad (11)$$

The kinetic devolatilization rate expression for the two competing rates (Kobayashi) model [24] is as given by the following equation:

$$\frac{m_v(t)}{(1 - f_{w,0}) m_{p,0}} = \int_0^t (\alpha_1 R_1 - \alpha_2 R_2) \left( \exp \left( - \int_0^t (R_1 - R_2) dt \right) \right) dt, \quad (12)$$

where  $m_v(t)$  is the volatile yield,  $f_{w,0}$  is the mass fraction of biomass,  $m_{p,0}$  is the initial particle mass at the injection boundary condition.  $R_1$  and  $R_2$  are the competing rates that control the devolatilization over various temperature range [24]:

$$R_1 = A_1 e^{-\frac{E}{RT}}, \quad (13)$$

$$R_2 = A_2 e^{-\frac{E}{RT}}, \quad (14)$$

where  $\alpha_1$ ,  $\alpha_2$  are the yield factors, and the value of  $\alpha_1$  is the mass fraction of volatile determined through the proximate analysis and  $\alpha_2$  is set as 1. Heat transfer during the devolatilization process are determined by the following equation

$$m_p c_p \frac{dT_p}{dt} = h A_p (T - T_p) + \frac{dm_p}{dt} h_{fg} + \epsilon_p A_p \sigma (T_R^4 - T_p^4), \quad (15)$$

where  $m_p$  is the mass of particle (kg), and  $c_p$  is the heat capacity of the particle (J/kg.K),  $T_p$  is the temperature of particle (K),  $h$  is the convective heat transfer coefficient (W/m<sup>2</sup>.K),  $A_p$  is the surface area of the particle (m<sup>2</sup>),  $h_{fg}$  is the latent heat (J/kg),  $\epsilon_p$  is the particle emissivity,  $\sigma$  is the Stefan Boltzmann constant ( $5.67 \times 10^{-8} \text{ kg s}^{-3} \text{ K}^{-4}$ ) and  $T_R$  is the radiation temperature (K). After the devolatilization process, char is formed and also volatile gases formed. Therefore, heat transfer during the char combustion/gasification process is derived by the following equation

$$m_p c_p \frac{dT_p}{dt} = h A_p (T - T_p) + f_h \frac{dm_p}{dt} H_{reaction} + \epsilon_p A_p \sigma (T_R^4 - T_p^4). \quad (16)$$

Finally, the particle temperature, convective heat transfer, and the absorption/emission of radiation of the particle surface are related by the following equation,

$$m_p c_p \frac{dT_p}{dt} = h A_p (T - T_p) + \epsilon_p A_p \sigma (T_R^4 - T_p^4). \quad (17)$$

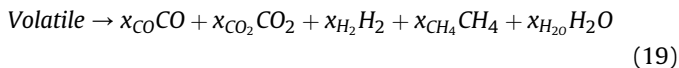
## 3. Models for biomass gasification: thermochemical kinetics

### 3.1. Reaction for pyrolysis

Pyrolysis is a thermochemical process that occurs in the absence of oxygen. Biomass (rubber wood in this case) fed into the gasifier first decomposes into char, volatile gases and tar:



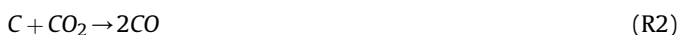
To calculate the volatile species, a volatile break-up scheme was used in our previously published work [22,25]. The model assumed that the volatile from biomass, consisting of carbon, hydrogen, oxygen, nitrogen and sulphur, converted to pseudo gas phase species, referred to as volatile using the devolatilization model:



However, tar is not considered in the CFD modelling due to its complex nature and remains outwith of the scope of this study. In reaction (19), the Stoichiometric coefficients  $x_{\text{CO}}$ ,  $x_{\text{CO}_2}$ ,  $x_{\text{H}_2}$ ,  $x_{\text{CH}_4}$  and  $x_{\text{H}_2\text{O}}$  for the resultant species are calculated from the mass fractions obtained through the ultimate and proximate analysis data, shown in Table 1, and considering the molecular weights of these species.

### 3.2. Heterogeneous (char) reactions

After devolatilization, char reacts with other volatile gases released from feedstock as well as with oxygen, which takes place in the oxidation zone. These reactions (R1-R4) shown in Table 2 are exothermic however, except the carbon oxygen reaction (combustion/oxidation reaction), the entire heterogeneous reactions take place in the reduction zone.



### 3.3. Homogenous reactions

For the gas phase reaction, CO, CO<sub>2</sub>, CH<sub>4</sub>, H<sub>2</sub>, N<sub>2</sub> and O<sub>2</sub> species are included in the simulation model, as presented below.



**Table 1**  
Chemical analysis data of rubber wood feedstock [26].

Proximate analysis (wt % dry basis)	
Volatile matter	81.1
Fixed carbon	19.2
Ash	0.7
Moisture content (wt % wet basis)	18.5
Ultimate analysis (wt% dry basis)	
C	50.6
H	6.5
O	42
N	0.2
S	0
Higher heating value (kJ/kg)	20540

**Table 2**  
Kinetics for the heterogeneous reactions [27].

Reactions	A	E (kJ/mol)	Temp (exponent)
R1: Partial oxidation	147000	112.99	1
R2: Boudouard Reaction	8.268	188.2	1
R3: Char-steam reaction	8.268	188.2	1
R4: Methanation reaction	8.88e-06	67.16	1

### 3.4. Numerical methods and simulation setup

The boundary conditions (mass flow inlet, pressure outlet, isothermal wall) for the simulations are the same as those used in the kinetic model [23]. The 3D CAD design and mesh domain of downdraft gasifier are shown in Fig. 2.

The operating conditions for the CFD simulation model are also shown in Table 4.

## 4. Results and discussion

As discussed above, CFD has been used to study the rubber wood gasification with the Eulerian-Lagrangian approach. Standard  $k-\epsilon$  model is used to take into account the gas phase turbulence while the DPM model to take into account the solid phase interactions. Initially, a CFD model is established according to the above simulation setup. The developed model is then validated by using the data from the experiment [26] and kinetic model [23]. Further, the study is extended to investigate the effects of various operating variables such as the gasifier temperature and equivalence ratio on the producer gas compositions (CO, CH<sub>4</sub>, CO<sub>2</sub>, H<sub>2</sub>, N<sub>2</sub>).

### 4.1. Grid independence test

Initially, a grid dependency on the simulated results has been performed considering a computational grid cell number of 215,012, 292,325, 418,685 and 666,707 respectively. The variation shown on the predicted results in Fig. 3 is very moderate, and in fact, a negligible difference is observed between the results obtained by 215,012 and 292,325. Hence, the grid of 215,012 is deemed to be the suitable one and thus chosen for all the other simulation cases presented in the following sections.

### 4.2. Cold flow analysis

Before looking into the gasification process in the gasifier, first, a

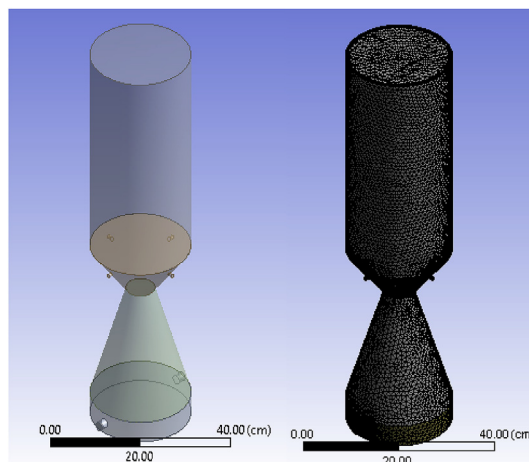


**Fig. 2.** 3D CAD design of downdraft gasifier and mesh domain.

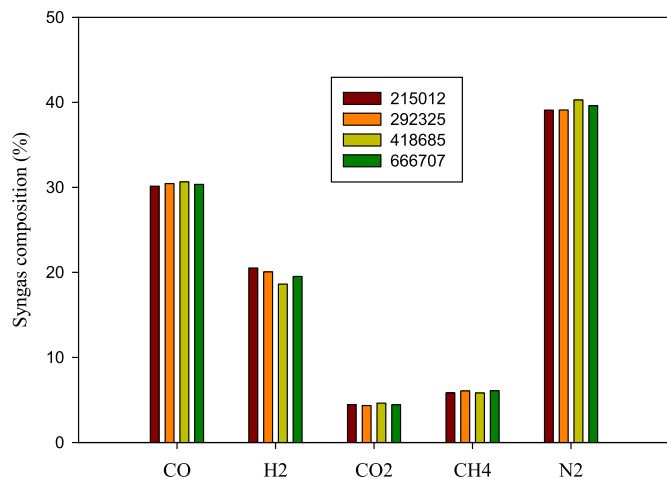


Fig. 3. Gas compositions at the gasifier outlet for different mesh sizes.

cold flow simulation is performed to check the flow velocity distribution (i.e. the hydrodynamics) and the fluid flow pattern inside the gasifier. The flow velocity magnitude and velocity vector distributions inside the downdraft gasifier are shown in Fig. 4.

For the injection of air, four nozzles are used as shown in Fig. 4, and the maximum air velocity is found at the entrance of the air nozzles. All the air released from the nozzles is directed towards the centre of the gasifier, and the velocity vectors also show that the air velocity magnitude near the nozzle of the wall is very less due to the wall boundary conditions employed. Following the understanding of the flow physics from the cold flow simulation, the energy conservation and species transport equations are included and solved simultaneously.

#### 4.3. Optimisation of the reaction kinetics for the homogeneous reactions

All the homogeneous reaction kinetics (Table 3) implemented into the CFD model resulted in the significant over-prediction of temperature inside the oxidation zone of the gasifier due to the exothermic nature of these reactions. This is a stumbling block for the CFD model to progress any further and hence, an in-depth sensitivity study on the kinetic parameters of the homogeneous reactions is deemed to be crucial in this respect. Literature [28]

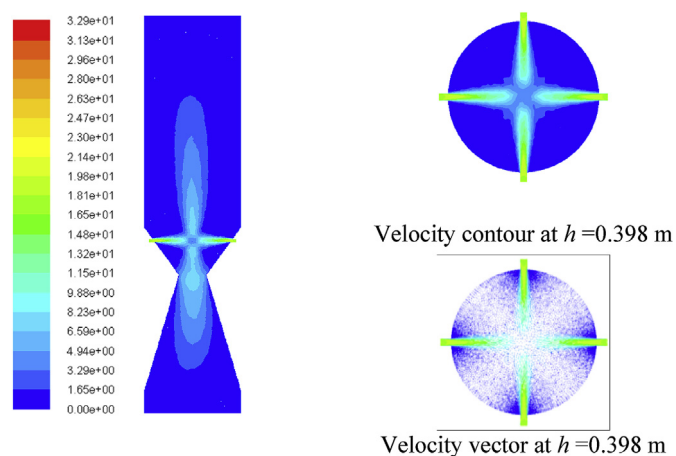


Fig. 4. Velocity magnitude and velocity vector distributions inside the downdraft gasifier.

Table 3  
Reaction kinetics for the homogeneous reactions [27,28].

Reactions	A	E (kJ/mol)	Temp (exponent)
Oxidation of CO	2.32e+12	167	0
Oxidation of H <sub>2</sub>	5.16e+13	28.5	0
Steam reforming reaction	2.8e+09	203	0
Water gas shift reaction	2.35e+10	288	0
Water gas shift reaction	1.78e+12	326	0
Methane reforming reaction	3.00e+05	125	0

suggests various reaction kinetic parameters for the homogeneous reactions ( $A$  and  $E$ ) as shown in Table 5, having a further variation in the frequency factor and activation energy even for the same reaction. Fig. 5 (a) shows the Arrhenius plots for the CO oxidation for the different chemical kinetics namely R5.1 to R5.5. This figure clearly points out the large discrepancies between the one set of kinetics to the another set. A close examination of Fig. 5 (a) also reveals that the lowest value of  $\ln(k)$  is obtained by R5 and the highest for R5.4. Further, Reaction R5 needs a lower activation energy to trigger the reaction compared to that of R5.4. Similarly, the Arrhenius plots for the combustion of hydrogen and methane and the steam-methane reforming are respectively presented in Fig. 5(b), (c) and (d).

Again, the effects of the kinetic parameters on the reaction rates for the hydrogen and methane combustion and the way the order of these reactions are controlled, based on the data sourced from the literature, are clearly evidenced through these results. This is further examined through the CFD model and the simulated results in terms of the maximum temperature are presented in Fig. 6.

It is understood that the maximum heat release from the homogeneous reactions occurs through the combustion of carbon monoxide. So, the investigation is firstly focused on the kinetics of this particular reaction with additional five different set of reaction parameters for R5.1 to R5.5 as shown in Table 5.

Further, from Fig. 6 it is observed that the highest maximum temperature in the oxidation zone is achieved from reaction R6.2, which is 2600 K. This temperature outcome is indeed very high for biomass gasification. To further investigate the consequence on the gasification temperature, different sets of reaction kinetics first for the oxidation of CO (R5- R5.5, as in Table 5) are simulated and the oxidation temperature is compared alongside. As shown in Fig. 6 again that the best agreed temperature result is obtained by R5 and in this context, this is considered to the optimised oxidation reaction for CO. Keeping this, the similar procedures were followed for the formation of water (R6 to R6.3) and oxidation of methane (R7 to R7.2). In addition, the steam reforming reaction was also included in the simulation, resulting in the optimised set of reaction kinetics that has the best agreed temperature. Table 6 finally presents these optimised reaction kinetics for the homogeneous reactions.

The temperature distributions inside the whole gasifier are presented in Fig. 7, as a set of contour plots, along both the radial and axial directions to assess the entire thermal field of the reactor.

Table 4  
Operating conditions for the CFD model.

Operating conditions	
Air flow rate (N.m <sup>3</sup> /hr)	1.64
Biomass feed rate (kg/hr)	3.65
Equivalence ratio (ER)	0.30–0.45
Pressure (atm)	1
Inlet air temperature (K)	600
Biomass feed temperature (K)	300

**Table 5**  
Reaction kinetics for various reactions.

Reaction kinetics for the oxidation of CO						
$\text{CO} + 0.5\text{O}_2 \rightarrow \text{CO}_2$ ; $r = Ae^{-E_a/(RT)}c_{\text{CO}}^x c_{\text{O}_2}^y c_{\text{H}_2\text{O}}^z$						
	x	y	z	$E_a$ (kJ/mol)	A	Ref.
R5	1	0.5	0.5	126	$1 \times 10^{10}$	[28]
R5.1	1	0.25	0.5	167	$2.32 \times 10^{12}$	[29]
R5.2	1	0.5	0.5	126	$1.30 \times 10^{11}$	[30]
R5.3	1	0.3	0.5	66.9	$4.78 \times 10^8$	[31]
R5.4	1	0.25	0.5	289	$1.28 \times 10^{17}$	[32]
R5.5	1	0.5	0.5	126	$3.25 \times 10^{10}$	[33]
Reaction kinetics for the formation of H <sub>2</sub> O						
$\text{H}_2 + 0.5\text{O}_2 \rightarrow \text{H}_2\text{O}$ ; $r = AT^ze^{-E_a/(RT)}c_{\text{H}_2}^x c_{\text{O}_2}^y$						
	x	y	z	$E_a$ (kJ/mol)	A	Ref.
R6	1	1	0	109	$2.20 \times 10^9$	[34]
R6.1	1.5	1	-1.5	28.5	$5.16 \times 10^{13}$	[28]
R6.2	1	1	0	125	$1.08 \times 10^{13}$	[35]
R6.3	1	1	0	42	$1.0 \times 10^{14}$	[14]
Reaction kinetics for the oxidation of CH <sub>4</sub>						
R7: $\text{CH}_4 + 0.5\text{O}_2 \rightarrow \text{CO} + 2\text{H}_2$						
R7.1: $\text{CH}_4 + 1.5\text{O}_2 \rightarrow \text{CO} + 2\text{H}_2\text{O}$ ; $r = AT^ze^{-E_a/(RT)}c_{\text{CH}_4}^x c_{\text{O}_2}^y$						
R7.2: $\text{CH}_4 + 2\text{O}_2 \rightarrow \text{CO}_2 + 2\text{H}_2\text{O}$						
	x	y	z	$E_a$ (kJ/mol)	A	Ref.
R7	0.5	1.25	0	126	$4.40 \times 10^{11}$	[36]
R7.1	-0.3	1.3	0	203	$2.80 \times 10^9$	[37]
R7.2	-0.3	1.3	0	203	$1.10 \times 10^9$	[37]
Reaction kinetics for the methane reforming reaction						
$\text{CH}_4 + \text{H}_2\text{O} \rightarrow \text{CO} + 3\text{H}_2$ ; $r = AT^ze^{-E_a/(RT)}c_{\text{CH}_4}^x c_{\text{H}_2\text{O}}^y$						
	x	y	z	$E_a$ (kJ/mol)	A	Ref.
R10	1	1	0	125	$3.00 \times 10^8$	[36]

As seen, the high-temperature regions are located at the oxidation zone due to the combustion reactions occurring above the air inlets, where the oxygen supply was adequate for combustion. The volatile gases, released from the pyrolysis zone, react with the oxygen available in this zone, and thus the maximum temperature zone is located there and the temperature near the air-nozzle regions is predicted to be lower. At the bottom of the gasifier (i.e. at  $h = 0$ ), the temperature range is 650–800 K which is a typical temperature of the gas releasing from the end of the reduction zone. While, towards the top of the gasifier, the temperature drops due to the heat required for both pyrolysis and drying of the biomass fed from the top of the gasifier initially at 300 K.

Fig. 8 presents a comparison of the simulated outlet composition of gases (CO, CO<sub>2</sub>, H<sub>2</sub>, CH<sub>4</sub>, and N<sub>2</sub>) with those obtained by the experimental testing and kinetic modelling results. These plots reveal that the simulated values of the outlet gas composition derived by the CFD model overestimate the gas composition of CO and CH<sub>4</sub>; whereas the comparison of H<sub>2</sub> and CO<sub>2</sub> seems to be reasonable but with an underproduction of N<sub>2</sub>. The model, however, does not include any tar species content and hence thought to possibly have some impacts on the overall comparison of the gas species as presented in this figure.

The model, therefore, converted all the tar contents with impurities into the syngas components, resulting the predicted gas composition of CO and CH<sub>4</sub> higher than those in the experimental and kinetic model. These findings corroborate with the results available in the literature [21]. Further, nitrogen presents in air as an inert gas and due to that, nitrogen does not take part in any reaction process during the gasification. In the biomass gasification, some nitrogen is liberated by pyrolysis, whereas in gas combustion, nitrogen oxides are formed from some of the nitrogen compounds at

temperature higher than that in gasification. Therefore, the unreactive nitrogen is passed through the gasification outlets with the producer gases and subsequently has an impact on the calorific value of the gases.

#### 4.4. Effects of operating parameters

In the biomass gasification, equivalence ratio is one of the most important operating parameters used to predict the process performance and design of gasifier. Fig. 9 illustrates the temperature profile along the gasifier height in the downdraft gasifier simulated at different equivalence ratios (ERs) changing from 0.30 to 0.45 at a constant biomass feed rate of 3.65 kg/h. As seen in Fig. 9, when the value of ER increases, the oxidation temperature increases due to an increase in the oxygen concentration. Subsequently, the char combustion and volatile combustion reactions (all are exothermic reactions) are triggered and as a result, temperature increases.

The predicted temperature was also in good agreement with that of the previously published results in the literature [38]. However, a significant drop in the temperature is examined in the pyrolysis zone. Drying and pyrolysis zone reactions are endothermic with a deficiency of heat. This heat deficiency recovers from the oxidation zone. Therefore, the process is linked with the endothermic drying, pyrolysis zone, and exothermic oxidation zone. In the oxidation zone, temperature increases and eventually becomes the highest due to the exothermic reactions occurring in this zone. In the reduction zone, mainly the endothermic reactions occur and, due to this, the temperature in the reduction zone drops.

Moreover, as seen in Fig. 10, the quality of gas obtained from the gasifier also strongly depends on the ER value. However, a relatively low value of the equivalence ratio may result in many problems, e.g.

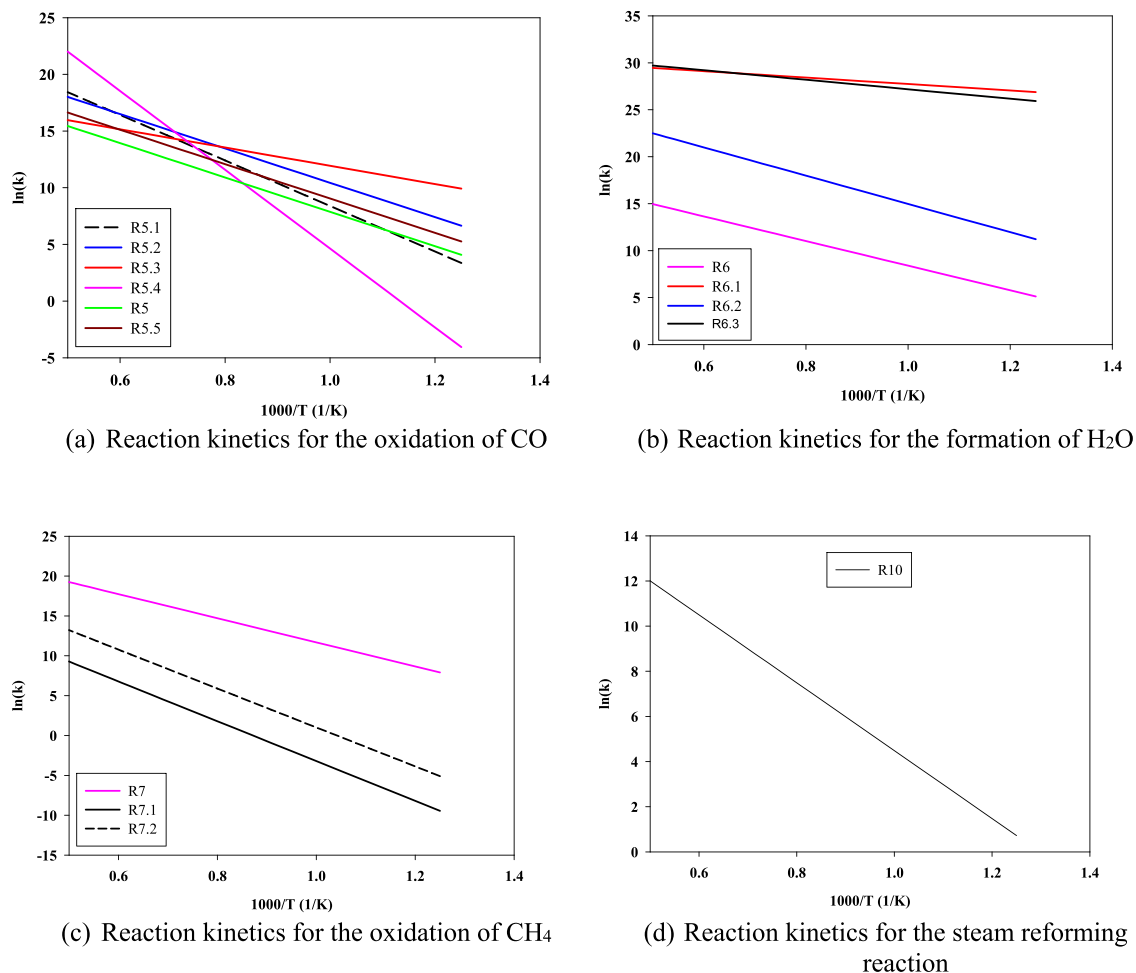


Fig. 5. Arrhenius rate coefficients for different reactions.

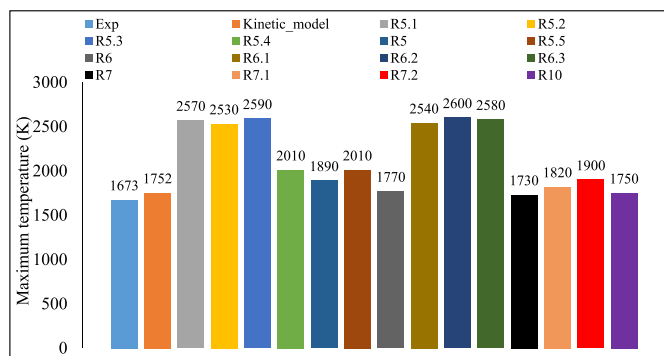


Fig. 6. Maximum temperature inside the downdraft gasifier for different reaction kinetics.

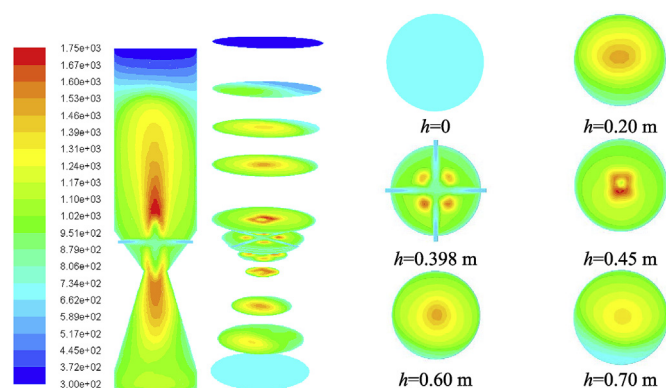


Fig. 7. Temperature profiles inside the downdraft gasifier.

Table 6 Optimised reaction kinetics for the homogenous reactions.

Optimised Reactions	A	E (kJ/mol)	Temp (exponent)
R5: Oxidation of CO	1e+10	126	0
R6: Oxidation of H <sub>2</sub>	2.2e+09	109	0
R7: Steam reforming reaction	4.4e+11	126	0
R10: Methane reforming reaction	3.0e+08	125	0

it may lead to a low heating value of gases produced with an excessive amount of char formation thus further resulting in an incomplete gasification. On the other side, a too large value of the equivalence ratio may result in an excessive formation of products through a complete combustion process. A close examination in Fig. 10 further shows that the methane mole fraction decreases with an increase of the equivalence ratio. However, on the other side, the mole fraction of carbon dioxide increases with the

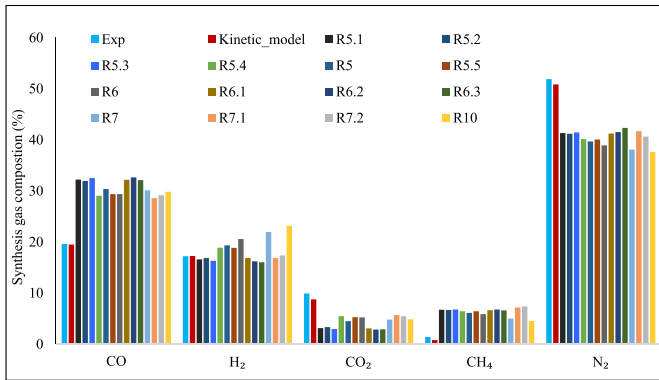


Fig. 8. Syngas compositions for different reaction kinetics.

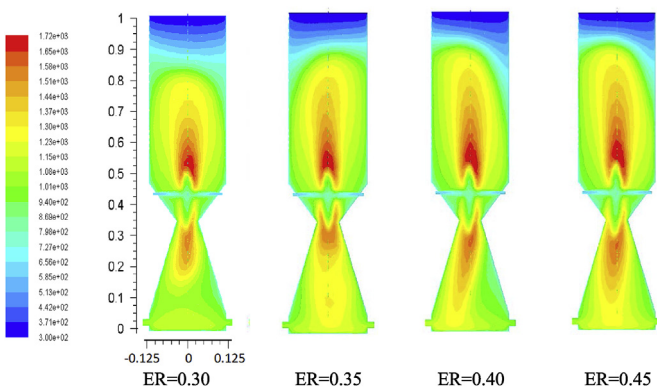


Fig. 9. Temperature distribution in the downdraft gasifier at various ERs.

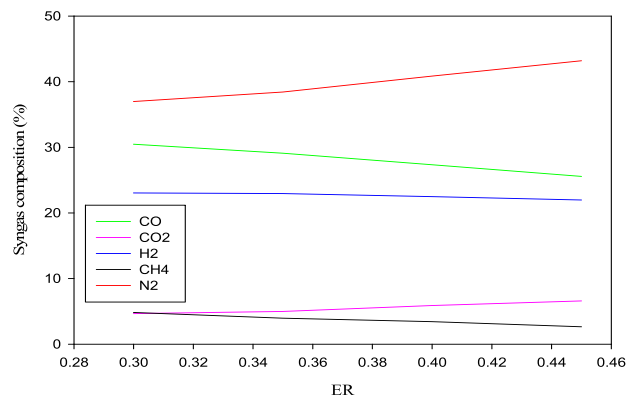


Fig. 10. Syngas composition at various ERs.

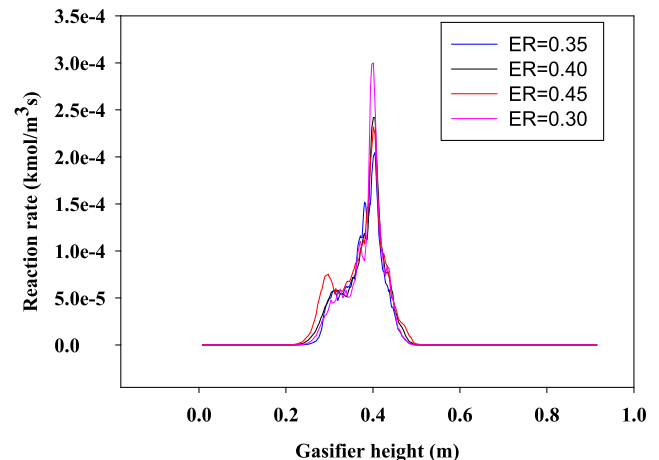
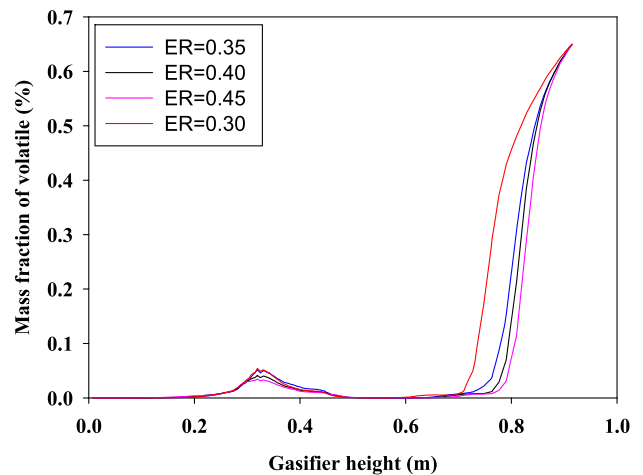


Fig. 11. (a) Mass fraction of volatile along the height of gasifier at various ER (top). (b) Reaction rate ( $2C + O_2 \rightarrow 2CO$ ) along the gasifier height at different ER.

from 0.6 m to the top (0.96 m) of the gasifier, which is the pyrolysis zone. For the higher ER, the volatile mass fraction rate is high due to the higher temperature in the oxidation zone. At a lower ER, the volatile mass fraction rate is low, compared to higher ERs.

Fig. 11(b) shows the reaction rate for the combustion reaction at various ERs along the gasifier height. The highest reaction rate is predicted in the oxidation zone for all the ERs. The highest reaction rate is for lower ER and the lowest reaction rate is for higher ER. This is due to the Le Chatelier's principle, which states that higher temperatures favour the formation of reactants in the exothermic reactions and also favour the formation of products through the endothermic reactions.

Fig. 12 finally presents the effects of the biomass feeding rate on the syngas production. It can be seen from Fig. 12 that the hydrogen concentration decreases while both the carbon monoxide concentration and methane concentration increase with the increasing biomass feed rate.

But carbon dioxide concentration remains almost constant for the various feed rates of rubber wood feedstock. This is due to the fact that when the mass flow rate of biomass for a fixed amount of air mass flow rate is increased, the temperature of gasifier decreases. However, the gasifier temperature as well as the formation of gas concentration in the gasifier is well described through the Le

equivalence ratio due to combustion, while the mole fraction of both carbon monoxide and hydrogen decreases with the equivalence ratio.

Fig. 11 (a) presents the decomposition of volatile matter mass fraction along the downdraft gasifier height at various ER ratios. When biomass enters from the top of the gasifier, due to the heat supplied by the oxidation zone it decomposes from higher molecules to volatile gases, char and tar. Further, the volatile gases reacted with char and converted into final product. Volatile matter decomposition takes place mostly in the pyrolysis zone as Fig. 11(a) clearly shows that all the volatile matter decomposed at a distance

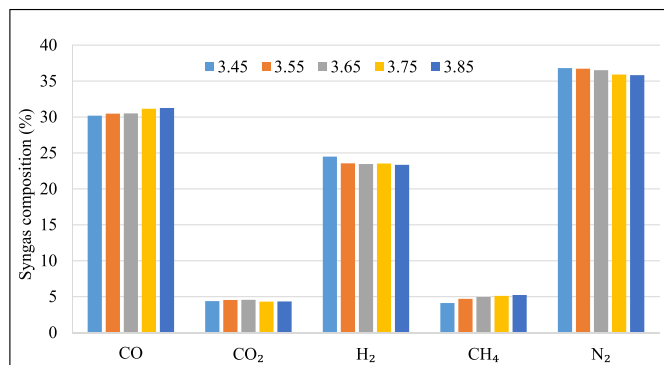


Fig. 12. Syngas composition at different biomass feed rates.

Chatelier's principle mentioned earlier. Therefore, the endothermic reaction (R10) is weakened with the temperature decrease, which further resulted in the decrease of H<sub>2</sub> concentration while increasing the CH<sub>4</sub> concentration with the increase of the biomass feeding rate. Moreover, the gas composition of CO is mainly determined through the exothermic reaction R1, thus the lower temperature is favourable for the CO production and consequently, the CO concentration also increases with the increase of biomass feeding rate.

## 5. Conclusions

A three-dimensional computational fluid dynamics (CFD) model was developed to study the gasification of biomass in a downdraft gasifier. Kinetic case study based on the homogeneous combustion reactions was carried out to optimise the gasifier temperature and syngas composition. Model validation was performed by comparing the predicted results of the gasifier temperature and syngas composition with those of the kinetic model and experimental data. As presented in the paper, the gasification results became very sensitive to the kinetics selection with the occurrence of the highest possible oxidation temperature of 2600 K from the reaction parameters utilised in R6.2 (oxidation of H<sub>2</sub>). The sensitivity study further revealed the optimised kinetic parameters for the homogeneous reactions consisting the oxidation of CO (R5), oxidation of H<sub>2</sub> (R6), steam reforming (R7) and methane reforming (R10). The oxidation zone temperature increased again when the equivalence ratio (ER) was increased from 0.3 to 0.45 as prompted by the oxidation reactions. However, when ER increased, carbon monoxide gas composition decreased but carbon dioxide increased. Furthermore, at a higher ER, the volatile release rate became fast compared to that of a lower ER. This model could potentially be used for industrial application for designing and optimising a downdraft gasifier and its syngas production. It could also be extended further by including a detailed tar model [39].

## Declaration of competing interest

The authors declare that they have no known competing financial interests or personal relationships that could have appeared to influence the work reported in this paper.

## Acknowledgement

We acknowledge Innovate UK (132362, TS/N011686/1) for the research grant support. The second author also acknowledges his RAEng/The Leverhulme Trust Senior Research Fellowship (LTSRF1718\14\45) provided by the Royal Academy of Engineering.

## References

- [1] U.S.E.I. Administration, International Energy Outlook 2016, Energy Information Administration (EIA), 2016.
- [2] M. La Villetta, M. Costa, N. Massarotti, Modelling approaches to biomass gasification: a review with emphasis on the stoichiometric method, *Renew. Sustain. Energy Rev.* 74 (2017) 71–88.
- [3] C.-H. Wang, D. Zhao, A. Tsutsumi, S. You, Sustainable energy technologies for energy saving and carbon emission reduction, *Appl. Energy* 194 (2017) 223–224.
- [4] A. Moharamian, S. Soltani, M.A. Rosen, S.M.S. Mahmoudi, T. Morosuk, A comparative thermoeconomic evaluation of three biomass and biomass-natural gas fired combined cycles using organic Rankine cycles, *J. Clean. Prod.* 161 (2017) 524–544.
- [5] O. Yucel, M.A. Hastaoglu, Kinetic modeling and simulation of throated downdraft gasifier, *Fuel Process. Technol.* 144 (2016) 145–154.
- [6] R.C. Sastry ABA, Biomass gasification processes in downdraft fixed bed reactors: a review, *Int. J. Chem. Eng. Appl.* 2 (2011) 425–433.
- [7] C. Chen, M. Horio, T. Kojima, Numerical simulation of entrained flow coal gasifiers. Part I: modeling of coal gasification in an entrained flow gasifier, *Chem. Eng. Sci.* 55 (2000) 3861–3874.
- [8] Z.A. Zainal, R. Ali, C.H. Lean, K.N. Seetharamu, Prediction of performance of a downdraft gasifier using equilibrium modeling for different biomass materials, *Energy Convers. Manag.* 42 (2001) 1499–1515.
- [9] A. Melgar, J.F. Pérez, H. Laget, A. Horillo, Thermochemical equilibrium modelling of a gasifying process, *Energy Convers. Manag.* 48 (2007) 59–67.
- [10] S. Jarungthammachote, A. Dutta, Thermodynamic equilibrium model and second law analysis of a downdraft waste gasifier, *Energy* 32 (2007) 1660–1669.
- [11] H.J. Huang, S. Ramaswamy, Modeling biomass gasification using thermodynamic equilibrium approach, *Appl. Biochem. Biotechnol.* 154 (2009) 14–25.
- [12] T.K. Patra, P.N. Sheth, Biomass gasification models for downdraft gasifier: a state-of-the-art review, *Renew. Sustain. Energy Rev.* 50 (2015) 583–593.
- [13] Y. Wang, C.M. Kinoshita, Kinetic model of biomass gasification, *Sol. Energy* 51 (1993) 19–25.
- [14] B. CD, Dynamic behaviour of stratified downdraft gasifiers, *Chem. Eng. Sci.* 55 (2000) 2931–2944.
- [15] Z. Ong, Y. Cheng, T. Maneerung, Z. Yao, Y.W. Tong, C.-H. Wang, et al., Co-gasification of woody biomass and sewage sludge in a fixed-bed downdraft gasifier, *AIChE J.* 61 (2015) 2508–2521.
- [16] D.F. Fletcher, B.S. Haynes, J. Chen, S.D. Joseph, Computational fluid dynamics modelling of an entrained flow biomass gasifier, *Appl. Math. Model.* 22 (1998) 747–757.
- [17] L. Gerun, M. Paraschiv, R. Vjue, J. Bellettre, M. Tazerout, B. Gøbel, et al., Numerical investigation of the partial oxidation in a two-stage downdraft gasifier, *Fuel* 87 (2008) 1383–1393.
- [18] K. Papadikis, S. Gu, A.V. Bridgwater, CFD modelling of the fast pyrolysis of biomass in fluidised bed reactors. Part B: heat, momentum and mass transport in bubbling fluidised beds, *Chem. Eng. Sci.* 64 (2009) 1036–1045.
- [19] Q. Xue, T.J. Heindel, R.O. Fox, A CFD model for biomass fast pyrolysis in fluidized-bed reactors, *Chem. Eng. Sci.* 66 (2011) 2440–2452.
- [20] H. Liu, A. Elkamel, A. Lohi, M. Biglari, Computational fluid dynamics modeling of biomass gasification in circulating fluidized-bed reactor using the eulerian–eulerian approach, *Ind. Eng. Chem. Res.* 52 (2013) 18162–18174.
- [21] Y. Wu, Q. Zhang, W. Yang, W. Blasiak, Two-dimensional computational fluid dynamics simulation of biomass gasification in a downdraft fixed-bed gasifier with highly preheated air and steam, *Energy Fuels* 27 (2013) 3274–3282.
- [22] U. Kumar, A.M. Salem, M.C. Paul, Investigating the thermochemical conversion of biomass in a downdraft gasifier with a volatile break-up approach, *Energy Procedia* 142 (2017) 822–828.
- [23] A.M. Salem, M.C. Paul, An integrated kinetic model for downdraft gasifier based on a novel approach that optimises the reduction zone of gasifier, *Biomass Bioenergy* 109 (2018) 172–181.
- [24] ANSYS 15 Fluent Theory Guide, Canonsburg, PA 15317, 2013.
- [25] U. Kumar, M.C. Paul, CFD modelling of biomass gasification with a volatile break-up approach, *Chem. Eng. Sci.* v195 (2019) pp413–pp422.
- [26] T.H. Jayah, L. Aye, R.J. Fuller, D.F. Stewart, Computer simulation of a downdraft wood gasifier for tea drying, *Biomass Bioenergy* 25 (2003) 459–469.
- [27] J. Xie, W. Zhong, B. Jin, Y. Shao, H. Liu, Simulation on gasification of forestry residues in fluidized beds by Eulerian–Lagrangian approach, *Bioresour. Technol.* 121 (2012) 36–46.
- [28] A. Gómez-Barea, B. Leckner, Modeling of biomass gasification in fluidized bed, *Prog. Energy Combust. Sci.* 36 (2010) 444–509.
- [29] F.L. Dryer, I. Glassman, High-temperature oxidation of CO and CH<sub>4</sub>, *Symp. (Int.) Combust.* 14 (1973) 987–1003.
- [30] J.B. Howard, G.C. Williams, D.H. Fine, Kinetics of carbon monoxide oxidation in postflame gases, *Symp. (Int.) Combust.* 14 (1973) 975–986.
- [31] H.C. Hottel, G.C. Williams, N.M. Nerheim, G.R. Schneider, Kinetic studies in stirred reactors: combustion of carbon monoxide and propane, *Symp. (Int.) Combust.* 10 (1965) 111–121.
- [32] R.A. Yetter, F.L. Dryer, H. Rabitz, Complications of one-step kinetics for moist CO oxidation, *Symp. (Int.) Combust.* 21 (1988) 749–760.
- [33] A. Jensen, J.E. Johnsson, J. Andries, K. Laughlin, G. Read, M. Mayer, et al., Formation and reduction of NO<sub>x</sub> in pressurized fluidized bed combustion of

- coal, *Fuel* 74 (1995) 1555–1569.
- [34] T. Mitani, F.A. Williams, Studies of cellular flames in hydrogen-oxygen-nitrogen mixtures, *Combust. Flame* 39 (1980) 169–190.
- [35] I. Petersen, J. Werther, Experimental investigation and modeling of gasification of sewage sludge in the circulating fluidized bed, *Chem. Eng. Process: Process Intensif.* 44 (2005) 717–736.
- [36] W.P. Jones, R.P. Lindstedt, Global reaction schemes for hydrocarbon combustion, *Combust. Flame* 73 (1988) 233–249.
- [37] C.K. Westbrook, F.L. Dryer, Chemical kinetic modeling of hydrocarbon combustion, *Prog. Energy Combust. Sci.* 10 (1984) 1–57.
- [38] I. Janajreh, M. Al Shraih, Numerical and experimental investigation of downdraft gasification of wood chips, *Energy Convers. Manag.* 65 (2013) 783–792.
- [39] A.M. Salem, I.N. Zaini, M.C. Paul, W. Yang, The evolution and formation of tar species in a downdraft gasifier: Numerical modelling and experimental validation, in: *Biomass and Bioenergy* 130, Pergamon, 2019, p. 105377.